# Persistent phosphor $SrAl_2O_4$:Eu,Dy in outdoor conditions: saved by the trap distribution

**Jonas Botterman[1,2] and Philippe F. Smet[1,2,*]**

[1] *LumiLab, Department of Solid State Sciences, Ghent University, Krijgslaan 281-S1, 9000 Ghent, Belgium*
[2] *Center for Nano- and Biophotonics (NB-Photonics), Ghent University, B-9000, Belgium*
[*] *philippe.smet@ugent.be*

**Abstract:** Persistent phosphors are a specific type of luminescent materials having the unique ability to emit light long after the excitation has ended. They are commonly used as emergency signage in near ideal, isothermal indoor situations. Recently, their energy storage capacity was relied on for outdoor situations, e.g. for glow-in-the-dark road marks and in combination with solar cells and photo catalytic processes. In this work the influence of temperature, illumination intensity and the duration of the night is critically evaluated on the performance of afterglow phosphors. The persistent luminescence of $SrAl_2O_4$:Eu,Dy green emitting phosphors is studied under realistic and idealized conditions. It is found that the light output profile is hardly influenced by the ambient temperature in a wide range. This is due to the presence of a broad trap depth distribution, which is beneficial to cover the longer and colder winter nights. Temperature drops during the night are however detrimental. For traffic applications, the total light output of glow-in-the-dark road marks at the end of the night is not sufficient for the studied compound, although re-charging by the car's headlamps partially alleviates this. For energy storage applications, the trap density should be improved and tunneling recombination processes might be needed to overcome overnight temperature drops.



**OCIS codes:** (260.3800) Luminescence; (300.6280) Spectroscopy, fluorescence and luminescence; (330.7310) Vision.

## References and links

1. L.-Y. Chen, W.-C. Cheng, C.-C. Tsai, J.-K. Chang, Y.-C. Huang, J.-C. Huang, and W.-H. Cheng, "Novel broadband glass phosphors for high CRI WLEDs," Opt. Express **22**(S3 Suppl 3), A671–A678 (2014).
2. J. Zhang and C. Jiang, "Photoluminescence properties of emission-tunable $Ca_8MgLa(PO_4)_7:Eu^{2+}$, $Mn^{2+}$ phosphors for white LEDs," Opt. Mater. Express **4**(10), 2102–2107 (2014).
3. A. Žukauskas, R. Vaicekauskas, P. Vitta, A. Zabiliūtė, A. Petrulis, and M. Shur, "Color rendition engineering of phosphor-converted light-emitting diodes," Opt. Express **21**(22), 26642–26656 (2013).
4. P. Leblans, D. Vandenbroucke, and P. Willems, "Storage phosphors for medical imaging," Materials (Basel) **4**(12), 1034–1086 (2011).
5. G. Krauss, S. Lohss, T. Hanke, A. Sell, S. Eggert, R. Huber, and A. Leitenstorfer, "Synthesis of a single cycle of light with compact erbium-doped fibre technology," Nat. Photonics **4**(1), 33–36 (2010).
6. K. Van den Eeckhout, P. F. Smet, and D. Poelman, "Persistent luminescence in $Eu^{2+}$-doped compounds: a review," Materials (Basel) **3**(4), 2536–2566 (2010).
7. M. Lastusaari, T. Laamanen, M. Malkamäki, K. O. Eskola, A. Kotlov, S. Carlson, E. Welter, H. F. Brito, M. Bettinelli, H. Jungner, and J. Hölsä, "The Bologna Stone: history's first persistent luminescent material," Eur. J. Mineral. **24**(5), 885–890 (2012).
8. T. Matsuzawa, Y. Aoki, N. Takeuchi, and Y. Murayama, "A new long phosphorescent phosphor with high brightness, $SrAl_2O_4:Eu^{2+},Dy^{3+}$," J. Electrochem. Soc. **143**(8), 2670–2673 (1996).
9. D. Poelman and P. F. Smet, "Photometry in the dark: time dependent visibility of low intensity light sources," Opt. Express **18**(25), 26293–26299 (2010).
10. Y. Miyamoto, H. Kato, Y. Honna, H. Yamamoto, and K. Ohmi, "An orange-emitting, long-persistent phosphor, $Ca_2Si_5N_8:Eu^{2+},Tm^{3+}$," J. Electrochem. Soc. **156**(9), J235–J241 (2009).

#237793 Received 9 Apr 2015; revised 9 Jun 2015; accepted 12 Jun 2015; published 23 Jun 2015

11. K. Van den Eeckhout, P. F. Smet, and D. Poelman, "Persistent luminescence in rare-earth codoped $Ca_2Si_5N_8:Eu^{2+}$," J. Lumin. **129**(10), 1140–1143 (2009).
12. P. F. Smet, J. Botterman, K. Van den Eeckhout, K. Korthout, and D. Poelman, "Persistent luminescence in nitride and oxynitride phosphors: A review," Opt. Mater. **36**(11), 1913–1919 (2014).
13. K. Van den Eeckhout, D. Poelman, and P. F. Smet, "Persistent luminescence in non-$Eu^{2+}$-doped compounds: a review," Materials (Basel) **6**(7), 2789–2818 (2013).
14. Z. Pan, Y.-Y. Lu, and F. Liu, "Sunlight-activated long-persistent luminescence in the near-infrared from $Cr^{(3+)}$-doped zinc gallogermanates," Nat. Mater. **11**(1), 58–63 (2012).
15. Y. Katayama, H. Kobayashi, and S. Tanabe, "Deep-red persistent luminescence in $Cr^{3+}$-doped $LaAlO_3$ perovskite phosphor for in vivo imaging," Appl. Phys. Express **8**(1), 012102 (2015).
16. Y. X. Zhuang, Y. Katayama, J. Ueda, and S. Tanabe, "A brief review on red to near-infrared persistent luminescence in transition-metal-activated phosphors," Opt. Mater. **36**(11), 1907–1912 (2014).
17. J. Ueda, T. Shinoda, and S. Tanabe, "Photochromism and near-infrared persistent luminescence in $Eu^{2+}$-$Nd^{3+}$-co-doped $CaAl_2O_4$ ceramics," Opt. Mater. Express **3**(6), 787–793 (2013).
18. F. Liu, W. Yan, Y.-J. Chuang, Z. Zhen, J. Xie, and Z. Pan, "Photostimulated near-infrared persistent luminescence as a new optical read-out from $Cr^{3+}$-doped $LiGa_5O_8$," Sci. Rep. **3**, 1554 (2013).
19. T. Maldiney, G. Sraiki, B. Viana, D. Gourier, C. Richard, D. Scherman, M. Bessodes, K. Van den Eeckhout, D. Poelman, and P. F. Smet, "In vivo optical imaging with rare earth doped $Ca_2Si_5N_8$ persistent luminescence nanoparticles," Opt. Mater. Express **2**(3), 261–268 (2012).
20. T. Maldiney, A. Bessière, J. Seguin, E. Teston, S. K. Sharma, B. Viana, A. J. J. Bos, P. Dorenbos, M. Bessodes, D. Gourier, D. Scherman, and C. Richard, "The in vivo activation of persistent nanophosphors for optical imaging of vascularization, tumours and grafted cells," Nat. Mater. **13**(4), 418–426 (2014).
21. Q. le Masne de Chermont, C. Chanéac, J. Seguin, F. Pellé, S. Maîtrejean, J.-P. Jolivet, D. Gourier, M. Bessodes, and D. Scherman, "Nanoprobes with near-infrared persistent luminescence for in vivo imaging," Proc. Natl. Acad. Sci. U.S.A. **104**(22), 9266–9271 (2007).
22. X. Ma, J. Zhang, H. Li, B. Duan, L. Guo, M. Que, and Y. Wang, "Violet blue long-lasting phosphorescence properties of Mg-doped $BaZrO_3$ and its ability to assist photocatalysis," J. Alloys Compd. **580**, 564–569 (2013).
23. Y. Mei, H. Xu, J. Zhang, Z. Ci, M. Duan, S. Peng, Z. Zhang, W. Tian, Y. Lu, and Y. Wang, "Design and spectral control of a novel ultraviolet emitting long lasting phosphor for assisting $TiO_2$ photocatalysis: $Zn_2SiO_4:Ga^{3+}$, $Bi^{3+}$," J. Alloys Compd. **622**, 908–912 (2015).
24. H. Sun, L. Pan, G. Zhu, X. Piao, L. Zhang, and Z. Sun, "Long afterglow $Sr_4Al_{14}O_{25}$:Eu,Dy phosphors as both scattering and down converting layer for CdS quantum dot-sensitized solar cells," Dalton Trans. **43**(40), 14936–14941 (2014).
25. K. Korthout, K. Van den Eeckhout, J. Botterman, S. Nikitenko, D. Poelman, and P. F. Smet, "Luminescence and x-ray absorption measurements of persistent $SrAl_2O_4$:Eu,Dy powders: Evidence for valence state changes," Phys. Rev. B **84**(8), 085140 (2011).
26. H. F. Brito, J. Holsa, T. Laamanen, M. Lastusaari, M. Malkamaki, and L. C. V. Rodrigues, "Persistent luminescence mechanisms: human imagination at work," Opt. Mater. Express **2**(4), 371–381 (2012).
27. P. F. Smet, K. Van den Eeckhout, A. J. J. Bos, E. van der Kolk, and P. Dorenbos, "Temperature and wavelength dependent trap filling in $M_2Si_5N_8$:Eu (M=Ca, Sr, Ba) persistent phosphors," J. Lumin. **132**(3), 682–689 (2012).
28. J. Botterman, J. J. Joos, and P. F. Smet, "Trapping and detrapping in $SrAl_2O_4$:Eu,Dy persistent phosphors: Influence of excitation wavelength and temperature," Phys. Rev. B **90**(8), 085147 (2014).
29. D. Poelman, N. Avci, and P. F. Smet, "Measured luminance and visual appearance of multi-color persistent phosphors," Opt. Express **17**(1), 358–364 (2009).
30. A. J. J. Bos, R. M. van Duijvenvoorde, E. van der Kolk, W. Drozdowski, and P. Dorenbos, "Thermoluminescence excitation spectroscopy: A versatile technique to study persistent luminescence phosphors," J. Lumin. **131**(7), 1465–1471 (2011).
31. C. Guo, L. Luan, D. Huang, Q. Su, and Y. Lv, "Study on the stability of phosphor $SrAl_2O_4:Eu^{2+}$, $Dy^{3+}$ in water and method to improve its moisture resistance," Mater. Chem. Phys. **106**(2-3), 268–272 (2007).
32. N. Avci, J. Musschoot, P. F. Smet, K. Korthout, A. Avci, C. Detavernier, and D. Poelman, "Microencapsulation of moisture-sensitive $CaS:Eu^{2+}$ particles with aluminum oxide," J. Electrochem. Soc. **156**(11), J333–J337 (2009).
33. C. A. Gueymard, "Interdisciplinary applications of a versatile spectral solar irradiance model: A review," Energy **30**(9), 1551–1576 (2005).
34. "CIE report. CIE191:2010 - Recommended System for Mesopic Photometry Based on Visual Performance (ISBN: 978 3 901906 88 6)."
35. A. Stockman and L. T. Sharpe, "Into the twilight zone: the complexities of mesopic vision and luminous efficiency," Ophthalmic Physiol. Opt. **26**(3), 225–239 (2006).
36. J. Ueda, K. Kuroishi, and S. Tanabe, "Bright persistent ceramic phosphors of $Ce^{3+}$-$Cr^{3+}$-codoped garnet able to store by blue light," Appl. Phys. Lett. **104**(10), 101904 (2014).
37. P. Dorenbos, "Mechanism of persistent luminescence in $Eu^{2+}$ and $Dy^{3+}$ codoped aluminate and silicate compounds," J. Electrochem. Soc. **152**(7), H107–H110 (2005).
38. K. Van den Eeckhout, A. J. J. Bos, D. Poelman, and P. F. Smet, "Revealing trap depth distributions in persistent phosphors," Phys. Rev. B **87**(4), 045126 (2013).
39. X. Long, J. He, J. Zhou, L. Fang, X. Zhou, F. Ren, and T. Xu, "A review on light-emitting diode based automotive headlamps," Renew. Sustain. Energy Rev. **41**, 29–41 (2015).


#237793 Received 9 Apr 2015; revised 9 Jun 2015; accepted 12 Jun 2015; published 23 Jun 2015

40. X. Shi, L. Shi, M. Li, J. Hou, L. Chen, C. Ye, W. Shen, L. Jiang, and Y. Song, "Efficient luminescence of long persistent phosphor combined with photonic crystal," ACS Appl. Mater. Interfaces **6**(9), 6317–6321 (2014).
41. A. Lecointre, A. Bessiere, A. J. J. Bos, P. Dorenbos, B. Viana, and S. Jacquart, "Designing a Red Persistent Luminescence Phosphor: The Example of $YPO_4:Pr^{3+},Ln^{3+}$ (Ln = Nd, Er, Ho, Dy)," J. Phys. Chem. C **115**(10), 4217–4227 (2011).
42. A. Dobrowolska, A. J. J. Bos, and P. Dorenbos, "Electron tunnelling phenomena in $YPO_4$: Ce, Ln (Ln = Er, Ho, Nd, Dy)," J. Phys. D Appl. Phys. **47**(33), 335301 (2014).
43. J. H. Oh, S. J. Yang, and Y. R. Do, "Healthy, natural, efficient and tunable lighting: four-package white LEDs for optimizing the circadian effect, color quality and vision performance," Light: Sci. Appl. **3**, e141 (2014).
44. Y. X. Zhuang, J. Ueda, and S. Tanabe, "Tunable trap depth in $Zn(Ga_{1-x}Al_x)_2O_4$:Cr,Bi red persistent phosphors: considerations of high-temperature persistent luminescence and photostimulated persistent luminescence," J. Mater. Chem. C **1**(47), 7849–7855 (2013).
45. A. Dombardt, U. Rohlfing, S. Weingaertner, K. Klinger, D. Kooss, K. Manz, and U. Lemmer, "New design tools for LED headlamps," Optical Sensors 2008 - SPIE, Proc. Soc. Photo Opt. Instrum. Eng. **7003**, 70032C (2008).
46. P. F. Smet, A. B. Parmentier, and D. Poelman, "Selecting conversion phosphors for white light-emitting diodes," J. Electrochem. Soc. **158**(6), R37–R54 (2011).

## 1. Introduction

Luminescent materials, often called phosphors, have a long tradition in lighting, displays and imaging techniques. Currently, luminescent materials provide a high quality emission spectrum to white LEDs [1–3], deliver crisp computed radiography images at lower irradiation dose [4] and power our light-based communications with rare earth doped (fiber) lasers [5]. A specific type of luminescence is persistent luminescence, also denoted as 'glow-in-the-dark', where the emission can continue for hours after the excitation ends [6]. Although the first reports in Europe date back to the early seventeenth century, describing a material now presumed to be copper doped barium sulfide [7], the main applications emerged with the introduction of ZnS:Cu,Co as green persistent phosphor and especially the much brighter $SrAl_2O_4:Eu^{2+},Dy^{3+}$ in 1994 [8]. Although these phosphors are nowadays commonly found in watch dials, toys and gadgets, their main application area is safety signage, e.g. as guiding strips in the aisle of an airplane and as emergency exit signage in ferries and buildings. This phosphor-based safety signage does not require electric wiring, consumes no electricity and is reliable in operation. The only prerequisite is a previous exposure to ambient light, which can easily be assumed. Upon a sudden power failure, the persistent phosphors provide sufficient light intensity to allow evacuation in a fully dark environment. Although the light intensity decreases quickly, initially following an exponential decay, the simultaneous dark adaptation of the human eye leads to an almost constant light perception in the first hour, with even an initial increase in perceived light intensity [9].

The research on persistent phosphors progressed mainly along two tracks in the past two decades. First of all, novel phosphor compositions were identified and optimized to provide strong persistent luminescence over a broader wavelength range. Nevertheless, $SrAl_2O_4:Eu^{2+},Dy^{3+}$ is still one of the best available compounds and good orange and red emitting phosphors are still lacking [10–13]. Strong progress was however made in phosphors emitting in the deep-red to near-infrared region of the spectrum [14–17]. They are often based on $Cr^{3+}$ or $Mn^{2+}$ and can provide very long afterglow durations [14, 18, 19]. The second track involved an exploration of other application areas. The use of persistent phosphors for in vivo bioimaging has been extensively demonstrated [20, 21], as well as the use of infrared emitting phosphors for night vision surveillance [14]. Besides these developments, the energy storage capacity of persistent phosphors has been explored for combined use with photo catalytic powders or with solar panels [22–24]. In both cases, the functionality (photocatalysis and power generation, respectively) is extended into the night time. As a step further from emergency signage, it was also proposed to use green emitting persistent phosphors as standalone road markings, obliterating the use of energy consuming street lighting. Clearly, there is a trend to move persistent phosphors towards outdoor applications.

The afterglow of $Eu^{2+}$-doped persistent phosphors relies on the thermal release of trapped electrons [25]. Although discussion remains on the exact trapping mechanisms at play in

#237793 Received 9 Apr 2015; revised 9 Jun 2015; accepted 12 Jun 2015; published 23 Jun 2015

persistent phosphors [26], these materials can be modelled by a number of trap states, characterized by a certain trap depth. Hence the phosphor's temperature during the afterglow can strongly affect its behavior, as shown in Fig. 1. As a consequence, glow-in-the-dark traffic markings might perform differently on cold winter nights and hot summer nights.

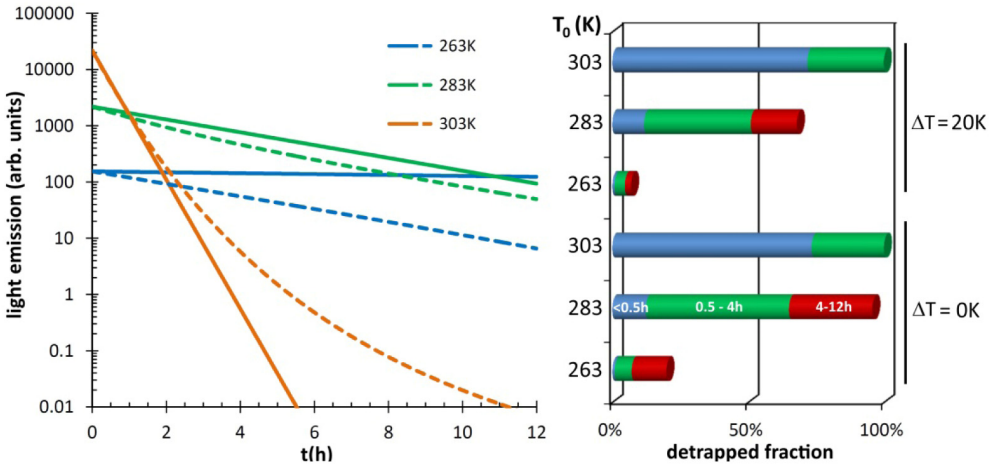


Fig. 1. (left) Simulated afterglow decay curves for a single, discrete trap depth of 0.85eV as function of the temperature, in the case of first order kinetics. Solid lines are for a fixed temperature (263K, 283K, 303K), dashed lines correspond to a linear temperature drop ΔT of 20K in 12h. (right) Fraction of the traps emptied during the first half hour (blue), between 0.5h and 4h (green) and between 4h and 12h (red) after ending the excitation, as function of the initial temperature $T_0$ and the temperature drop ΔT.

In the case of a single discrete trap depth, relatively small changes in temperature have a large impact on the afterglow profile (Fig. 1). Higher temperature gives a high initial brightness, but leads to a quick brightness decrease due to a fast detrapping. At lower temperature, the light output is more stable in terms of intensity. The overall light intensity is however rather low, and only a limited number of traps are emptied, even after 12h. A temperature drop during the night has also a strong influence on the detrapping characteristic. Clearly, if this particular hypothetical material is to be used in outdoor conditions with natural temperature variations, then the performance will not be consistent.

Also the day time temperature might have its repercussions on the afterglow performance during the night. When temperature is too high during charging, this results in almost immediate emptying of the traps relevant for afterglow upon filling them. At low temperature the filling of traps in the phosphors can be hampered if a thermal barrier for trapping is present [27, 28]. Additionally, the excitation intensity during the day, determined by the solar irradiance, influences the number of filled traps in the phosphor. On clear sunny days more traps in the phosphor might get filled than compared to the number of filled traps after a grey or foggy day.

It is clear that before stating that persistent luminescent phosphors can effectively be used in glow-in-the-dark traffic markings, a thorough feasibility study must be performed. Here the use of $SrAl_2O_4:Eu^{2+},Dy^{3+}$ in glow-in-the-dark traffic markings is investigated, for which important parameters such as day and night temperature variations, excitation conditions and length of the night are taken into account.

In principle this study could be performed outside, although one is then restricted to the outdoor conditions of that specific day. Therefore we performed these measurements using a modified thermoluminescence setup, able to simulate arbitrary temperature profiles and excitation intensities. Realistic day and night outdoor conditions can then be mimicked while retaining the flexibility of performing the experiments. Representative days and nights during

#237793 Received 9 Apr 2015; revised 9 Jun 2015; accepted 12 Jun 2015; published 23 Jun 2015

summer and winter were simulated using input data provided by a local weather station. In addition, idealized day and night profiles were simulated along with dedicated TL measurements to be able to draw a more general conclusion on the overall feasibility.

## 2. Materials and methods

All measurements were performed on a thin, pressed pellet of $SrAl_2O_4:Eu^{2+},Dy^{3+}$ powder (GloTech International). Powder X-ray diffraction (XRD) measurement confirmed that the powder is pure phase (ICSD No. 26466) without traces of other crystalline products (data not shown).

$SrAl_2O_4:Eu^{2+},Dy^{3+}$ emits the typical green light of most commercial glow-in-the-dark gadgets. The emission spectrum around room temperature shows a characteristic broad $Eu^{2+}$ based emission band with a maximum at 520nm and a full width at half maximum (FWHM) of about 85nm (Fig. 2) [28]. These emission characteristics are close to ideal for glow-in-the-dark applications as the human eye is very sensitive to this light in both photopic and scotopic vision mode [29].

A modified thermoluminescence setup was used to investigate the phosphor's behavior under simulated variable temperature and illumination conditions [28]. The temperature controller was programmed to instantaneously adjust the sample temperature to the input temperature, provided by weather station data or idealized temperature curves. A 395nm LED (FWHM of 17nm) was chosen as the excitation source as its emission spectrum is located near the maximum of the excitation spectrum of the persistent luminescence for $SrAl_2O_4:Eu^{2+},Dy^{3+}$ [30]. In addition, the spectral distance allowed to easily separate the persistent luminescence from the reflected excitation light by means of an Acton SP2300 monochromator (Princeton Instruments) combined with a ProEM1600 EMCCD camera. The light collection efficiency was calibrated by a calibrated photometer (ILT 1700, International Light Technologies).

Practical aspects (shadow, dirt, snow coverage…) of traffic markings are not taken into account in this study, and the obtained brightness profiles can be considered as the most favorable situation.

It is known that $SrAl_2O_4:Eu^{2+},Dy^{3+}$ shows degradation in the presence of water [31]. After storing the phosphor used in this study in water for two years, its persistent luminescence had decreased by more than 50% [12], which might hamper its use in outdoor applications. Here we do not discuss this degradation and assume the phosphor to be stable, which can be achieved by proper encapsulation, surface modification or by embedding in an impermeable matrix [31, 32].

## 3. Results and discussion

### *3.1. Meteorological conditions*

Whereas the temperature for indoor applications of persistent phosphors remains quasi constant during excitation and afterglow, this is certainly not the case outdoor. Obviously, the temperature will commonly be higher during daytime charging than during the afterglow phase at night. Not only fluctuations in temperature during day and night, but also the large temperature difference between different seasons should be taken into account.

In outdoor applications, charging of persistent phosphors relies on solar illumination. However, not all of the light irradiated by the sun is useful to charge these phosphors. In case of $SrAl_2O_4:Eu^{2+},Dy^{3+}$, Bos et al. performed thermoluminescence-excitation spectroscopy measurements, from which the excitation spectrum for the persistent luminescence was deduced [30]. Only photons with wavelength shorter than 450nm are able to efficiently fill traps in $SrAl_2O_4:Eu^{2+},Dy^{3+}$, which amounts to about 14% of the incident solar spectrum at the top of the atmosphere (Fig. 2). However, sunlight has to traverse the earth's atmosphere where wavelength dependent absorption and scattering (Rayleigh scattering as well as Mie

#237793 Received 9 Apr 2015; revised 9 Jun 2015; accepted 12 Jun 2015; published 23 Jun 2015

scattering at larger particles) take place, modifying the spectrum of the sunlight that eventually reaches the earth's surface. Moreover, the spectrum of sunlight incident on the earth's surface also changes as a function of place, date and time, as these parameters all influence the solar elevation and the distance travelled by the sunlight through the atmosphere. A decent understanding of how atmospheric effects alter the solar spectrum during the day is required when trying to mimic the charging of a phosphor.

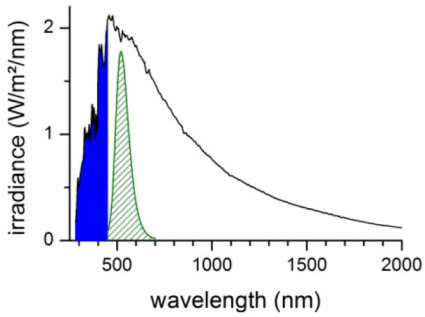


Fig. 2. (black trace) Extraterrestrial solar spectral irradiance (AM0) [33]. The sun emits light with wavelengths ranging from 270 to 4000nm, with about 14% of the irradiated solar power originating from light with $\lambda < 450$nm (blue area). The emission spectrum of $SrAl_2O_4$:Eu,Dy is shown as the green overlay.

To evaluate the fraction of solar irradiance *E* with wavelengths shorter than 450nm, received on a specific surface on earth, the SMARTS code was used [33], which is able to simulate the atmospheric effects on the solar spectrum on every date and time for every place on earth. The details are elaborated in Appendix A. With the code, the global irradiance on a horizontal surface (GHI) can be determined, which is the most relevant parameter for road marks. From these spectra, the fraction $f_{\lambda<450nm}$ of the irradiance corresponding to light with $\lambda < 450$nm can be derived. About 12% of the sun light incident on a surface horizontal to the ground is useful to charge $SrAl_2O_4:Eu^{2+},Dy^{3+}$. This value shows only a limited seasonal variation, so that the use of a fixed value is justified. Consequently, a fraction equal to 12% of the GHI values can be taken as input data for the simulations on $SrAl_2O_4:Eu^{2+},Dy^{3+}$. GHI values are available from local weather stations equipped with a pyranometer yielding the solar radiation flux density (in $W/m^2$) from a field of view of 180°.

### *3.2. Simulated day and nights*

Selected days and nights were simulated with input data provided by a local weather station in Belgium. The GHI and temperature variation used as input for these experiments are shown in Fig. 3. The data have been shifted such that the moment of highest solar elevation is at 12:00 to ease interpretation. For July 6, 2012 GHI values of about $1000W/m^2$ are reached when the Sun is at the highest position [Fig. 3(a)]. The large fluctuations originate from vast cloud formation. The outdoor temperature fluctuates between 288K and 298K and there is a clear correlation between the GHI and the outdoor temperature. Figure 3 (b) shows meteorological data of January 16, 2013. During this winter's day and night the GHI reaches maximal values of only $250W/m^2$ and the outdoor temperature fluctuates between 263K and 273K.

These meteorological input data (temperature and solar irradiation) were subsequently translated to the experimental setup. The current through the 395nm pumping LED was driven by the programmable power supply in a way that the sample was illuminated with an irradiance corresponding to 12% of the GHI values extracted from the meteorological data. Light emitted by the $SrAl_2O_4:Eu^{2+},Dy^{3+}$ sample is recorded during the entire 'simulated' day and night [Figs. 3(c) and (d)]. Note that the luminance (in $cd/m^2$) on the vertical axes of both figures is plotted on a logarithmic scale. The emitted intensity from the phosphor during

#237793 Received 9 Apr 2015; revised 9 Jun 2015; accepted 12 Jun 2015; published 23 Jun 2015

illumination is in line with the intensity fluctuations of the excitation source and the gradually diminishing solar irradiance. This measured emission intensity is the result of both steady state photoluminescence and afterglow emission during the illumination [28]. Note that illumination with the full solar spectrum would lead to a much higher daytime luminance due to the reflection of visible light not absorbed by the phosphor.

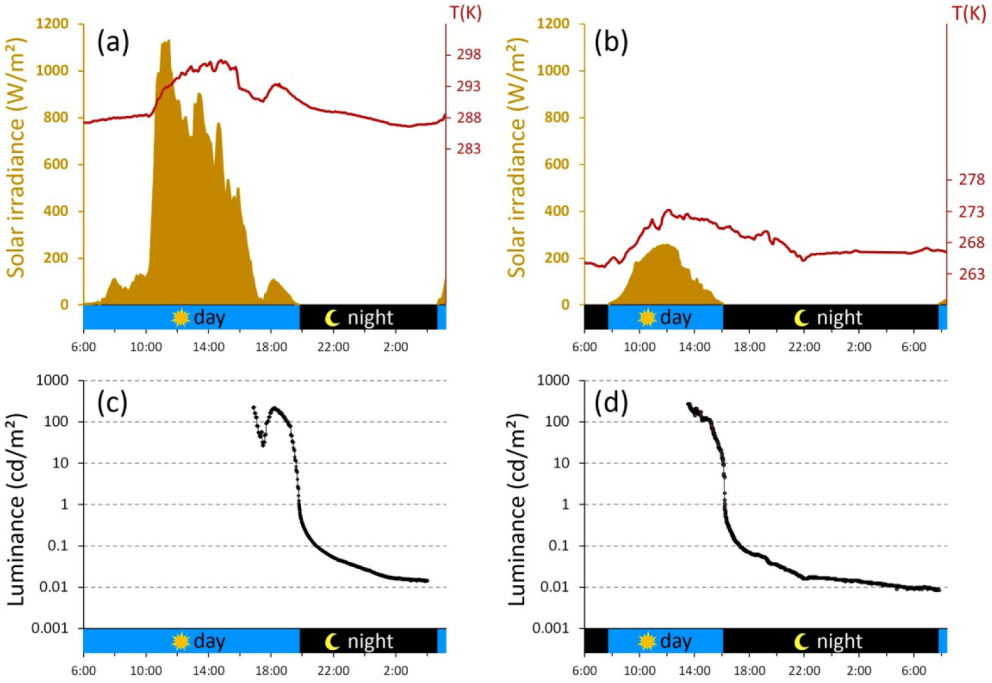


Fig. 3. Solar irradiance data (orange) and temperature data (red) on July 6, 2012 (a) and on January 16, 2013 (b).The data, obtained from a weather station in Knokke-Heist (Belgium), have been shifted such that the moment of highest solar elevation is at 12:00. The data were used as input to mimic real day and night conditions in our setup. Luminance profiles (c) and (d) for the luminescence of the $SrAl_2O_4:Eu^{2+},Dy^{3+}$ phosphor corresponding to the irradiance and temperature profiles (a) and (b), respectively.

When the excitation source is completely switched off and the steady state photoluminescence has ceased, then all the measured light is solely attributed to afterglow emission. For both nights, the afterglow emission starts with an initial intensity of around 1cd/m$^2$ after which it decays quickly. The afterglow intensity decreases an order of magnitude within the first hour of darkness and another order of magnitude during the remainder of the night. Changes in the outdoor temperature during the night are reflected instantaneously in the measured luminance. When temperature drops, the afterglow intensity decreases faster, while an increase in temperature results in a more steady afterglow intensity. Especially in the results from the winter's night simulation, where the fluctuations in temperature are more pronounced, these effects can be seen. As an example, compare Figs. 3(b) and (d) around 22:00.

The afterglow is measureable throughout the entire night, however the intensity is fairly low during most of the night. On both simulated nights, the emission intensity starts at approximately the same value and, although the winter's night is much colder, the intensity overnight remains comparable. At the end of the night the luminance is almost the same, despite the large difference in duration. Furthermore, the temperature evolution during the night also plays a role. During this specific summer's night the temperature decreases monotonically, leading to a slightly faster decrease of the afterglow intensity, while during

#237793 Received 9 Apr 2015; revised 9 Jun 2015; accepted 12 Jun 2015; published 23 Jun 2015

the simulated winter's night the temperature remains stable or even increases in this particular simulation, leading to a slower decrease of the afterglow intensity during that night. It can be expected that the differences in afterglow performance of the persistent phosphor will be more pronounced when comparing extremely hot and cold nights, or when comparing nights with constant temperature and strongly decreasing temperature.

The measured luminance values should however be translated in terms of visibility. In assessing persistent phosphors, a value of 0.3mcd/$m^2$ is often used as a visibility threshold. This value is about 100 times the sensitivity of a fully dark adapted human eye [29]. However, this threshold value is rather meaningless in this specific outdoor application for several reasons. Firstly, this limit is set for a light source in a completely dark environment, whereas it is hardly ever completely dark outdoor. Secondly, the eye of a human road user is never at its highest sensitivity as it cannot get fully dark adapted [34], due to moonlight, dashboard illumination, headlamps of other road users, etc. To evaluate the performance of outdoor applications such as glow-in-the-dark traffic markings one could use a different criterion such as target contrast, being the relative luminance difference between the target and its background. In case of glow-in-the-dark traffic markings, the luminance of the background consist of the reflection on the road surface of moonlight and other light sources along the road. The luminance of the target will be the sum of the light emitted by the afterglow phosphor, i.e. what was measured in the experiment, and the reflection on the traffic markings of the ambient light. In order to achieve a good target contrast value, the luminance of the target must be significantly larger than the background luminance. Considering the typical luminance of the road surface upon full moon being of the order of 0.1cd/$m^2$ [35], one notices that the persistent phosphor quickly drops below this level. Clearly, the total number of thermally accessible traps should be increased, or the effective thickness of the phosphor layer should be increased, e.g. by embedding into a translucent matrix or using thicker ceramic-like phosphors [36], to lift the luminance at the end of the night into the 0.1 to 1 cd/$m^2$ region.

### *3.3. Idealized temperature profiles*

To gain insight in the evolution of the afterglow with variable temperature a number of hypothetical nights with idealized temperature profiles were simulated. These nights have a duration of 12h and the idealized temperature profile starts at temperature $T_0$ and drops $\Delta T$ degrees over the timespan of 12h along a quarter of a sine function. Prior to the beginning of the night, the $SrAl_2O_4:Eu^{2+},Dy^{3+}$ sample is excited using a 395nm LED for which the output power is programmed to mimic a sunset starting at a solar irradiance of 25W/$m^2$, and decreasing linearly in one hour to 0W/$m^2$. For this particular phosphor, longer irradiation times starting at higher irradiance did not result in a substantial increase in the afterglow. A series of measurements with $T_0$ values of 303K, 293K, 283K and 273K and $\Delta T$ values of 0K, 10K and 20K were conducted. Although the temperature was programmed to decrease over a timespan of 12h, the afterglow intensity is only shown until 7h after the end of the excitation, reason being the very low levels of afterglow in some cases after less than 7h (Fig. 4).

The integrated luminance at $t < 0$h is the sum of steady state photoluminescence and afterglow from the phosphor upon excitation. At $t = 0$h, the excitation source is completely switched off and the integrated emission intensity solely consists of afterglow from the $SrAl_2O_4:Eu^{2+},Dy^{3+}$ phosphor. When comparing the four graphs in Fig. 4, they appear surprisingly similar. The emission intensity profile is nearly the same for each $T_0$ value, which is in strong contrast to the temperature dependent behavior of the single trap assumption (Fig. 1). The phosphor performs best if the temperature doesn't decrease during the night (i.e. $\Delta T = 0$K), which is observed for the entire studied range of initial temperatures. With increasing $\Delta T$ values the afterglow luminance lowers significantly after a few hours into the night compared to the case of a stable temperature. Also, a few subtle yet crucial differences are noticeable, related to the initial temperature $T_0$. Comparing the afterglow

#237793 Received 9 Apr 2015; revised 9 Jun 2015; accepted 12 Jun 2015; published 23 Jun 2015

curves for which ΔT = 0K (red curves), one can see that the luminance increases with decreasing $T_0$ value after a few hours into the night.

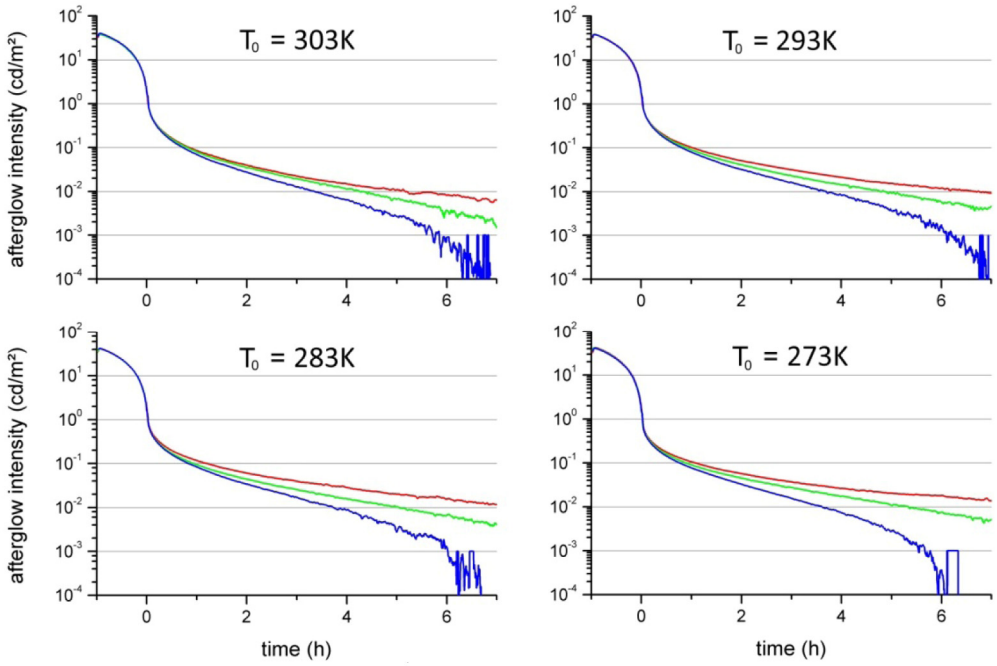


Fig. 4. Afterglow intensity of $SrAl_2O_4:Eu^{2+},Dy^{3+}$ as a function of time during the `idealized' nights. The red, green and blue curves show the results for nights with temperature drops ΔT = 0K, 10K and 20K, respectively. Time $t$ = 0h corresponds to sunset (i.e. the end of the excitation).

### *3.4. Thermoluminescence*

By recording a thermoluminescence glow curve after the afterglow measurement (as in Fig. 4), the number of traps that remain filled after 7 hours of darkness can be evaluated, as well as their depth distribution. Selected TL glow curves are plotted in Fig. 5. For clarity, the TL glow curves measured after 7h of afterglow for $T_0$ = 273K and 303K only are shown and for the cases with a stable temperature overnight (ΔT = 0K) and with a significant temperature drop (ΔT = 20K). In addition, TL measurements were also performed immediately after the end of the excitation at 303K and at 273K (i.e. without the afterglow phase). From the shape and position of these TL curves, it is clear that a rather broad trap depth distribution is present, with some substructure clearly visible. The origin of the different trap depths in $SrAl_2O_4$:Eu,Dy, and their contribution in the trap distribution, is still under discussion [6, 26, 37]. They are presumably not only related to the presence of intrinsic traps (e.g. oxygen vacancies), as the addition of co-dopants (e.g. $Dy^{3+}$) also leads to additional trap centers. Although assigning the different contributions in the glow curves to particular defect centers is out of the scope of this paper, it is known that by appropriate tuning of the synthesis conditions more favorable trap distributions might be obtained. In any case, these TL curves recorded before the start of the afterglow provide key information about the distribution of filled traps at the beginning of the night. Notice that the TL glow curves coincide on the high temperature side. The TL maximum shifts as function of the temperature during charging, which is a telltale sign for the presence of a trap distribution [38].

From the TL curves in Fig. 5 several characteristics can be deduced. First of all, comparing the solid curves it can be seen that significantly more traps are filled after charging the phosphor at 273K (blue solid curve) than after charging at 303K (red curve). Large

#237793 Received 9 Apr 2015; revised 9 Jun 2015; accepted 12 Jun 2015; published 23 Jun 2015

fraction of the traps which were filled after charging at 273K can be considered being too shallow at 303K, i.e. they are continuously filled and emptied, due to the availability of significantly more thermal energy. Consequently, the maximum in the TL curves shifts to higher temperature. At the start of a night, more energy is thus stored in the phosphor at low temperature and thus potentially more light can be emitted during the night. Secondly, when comparing the dashed curves with the dotted curves, it can be seen that more traps remain filled after 7h of afterglow when the temperature decreases overnight, both for $T_0$ = 273K and $T_0$ = 303K. This is not unexpected, as a decrease in temperature implies that less thermal energy is available to release trapped electrons and thus more traps remain filled. This result is also in line with the lower afterglow intensity for overnight decreasing temperatures (Fig. 4).

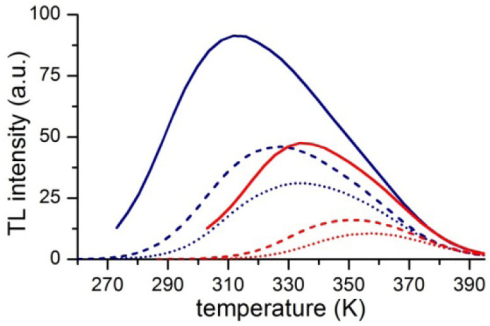


Fig. 5. TL glow curves measured after 7h of afterglow for $T_0$ = 303K with $\Delta T$ = 0K (red dotted curve) and $\Delta T$ = 20K (red dashed curve). TL glow curve measured immediately after ending the excitation at $T_0$ = 303K (solid red curve). Similarly for $T_0$ = 273K (blue curves).

From the TL curves it is also clear that for warm summer nights almost all traps are emptied after 7h, somewhat depending on the temperature evolution. For colder nights a considerably larger number of traps is still filled after 7h, which is favourable to span the longer duration of a winter night (up to 16h for a latitude of 50°), provided the temperature drop is not too severe overnight. Actually, the broad trap depth distribution in $SrAl_2O_4:Eu^{2+},Dy^{3+}$ results in afterglow from the phosphor in a rather large temperature range. In case of a more narrow trap depth distribution, the difference in afterglow intensity between a warm and cold night would be much larger, similar to the case in Fig. 1.

### *3.5. Additional charging by headlamps*

The broad trap depth distribution in $SrAl_2O_4:Eu^{2+},Dy^{3+}$ is advantageous to have a more or less similar detrapping behavior, irrespective of the temperature. In addition, during winter nights more energy was stored in the phosphor allowing to span the longer winter nights. However the light emission from the phosphor is currently not sufficient after a few hours of darkness, especially if temperature drops considerably during the night. Additional charging of the phosphor during the night might overcome these issues, e.g. by the headlamps of motorized traffic.

To evaluate to what extent glow-in-the-dark traffic markings could be additionally charged by passing cars, it should be known how long and intense the traffic markings are lit by the headlamps of a car passing by. The speed of the car, the stretch of the road lit by the headlamps and the intensity and spectral distribution emitted by the headlamps are the key parameters. The calculations are detailed in Appendix B. The spectral fraction of headlamps' emission being useful to charge the $SrAl_2O_4$:Eu,Dy phosphor was estimated at 10%, which is an overestimation for tungsten-halogen lamps but rather realistic for the emerging LED based headlamps having a higher correlated color temperature [39].

#237793 Received 9 Apr 2015; revised 9 Jun 2015; accepted 12 Jun 2015; published 23 Jun 2015

Due to technical limitations, the illumination by the headlamps was simulated for bunches of 30 cars, rather than for individual cars passing by (Fig. 6), which makes no difference to the overall charging the $SrAl_2O_4$:Eu,Dy phosphor.

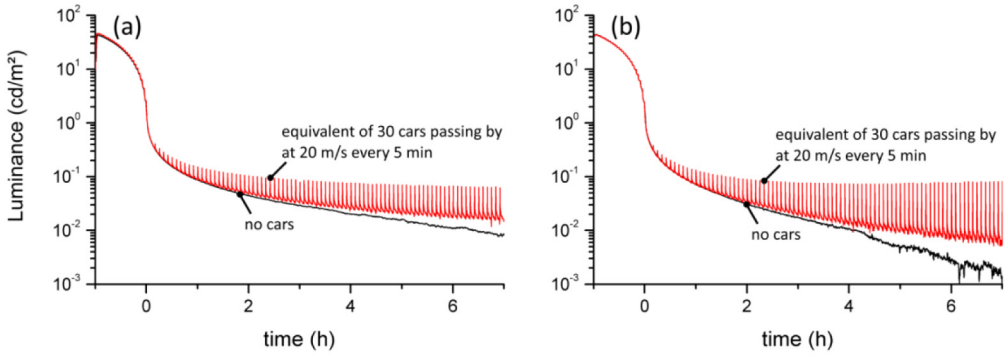


Fig. 6. Comparison of the afterglow intensity of $SrAl_2O_4$:Eu,Dy without (black curve) and with (red curve) additional charging by cars headlamps during the night. (a) $T_0$ = 293K and $\Delta T$ = 0K. (b) $T_0$ = 293K and $\Delta T$ = 20K.

The equivalence of 30 cars driving by at 20m/s every 5 minutes (i.e. 1 car every 10s) was compared to the situation without additional charging by traffic. For an initial temperature $T_0$ of 293K, both situations of steady temperature and a temperature drop of 20K were modelled.

The luminance shows a sharp increase in intensity every time a bunch of cars passed by, partially due to the steady state luminescence. The intensity drops back almost immediately to the intensity profile in the absence of passing cars. It is only after a few hours into the night that an appreciable increase in afterglow intensity can be noticed. This overall increase in intensity is limited and it must be noted that the density of cars at night in these simulations is rather elevated. In the case of a steadily dropping temperature, the effect of the additional charging is more pronounced [Fig. 6(b)] as less deep, and thus more accessible, traps become filled.

It can thus be concluded that additional charging by light from the headlamps of passing cars is possible, yet insufficient to fully overcome the low afterglow intensity in the later stages of the night. This is due to the rather low illuminance on the road by the headlamps on the one hand and the limited amount of useful short wavelength light on the other hand.

### *3.6. From simulation to application*

Upon application of a specific persistent phosphor in outdoor conditions, one should consider the daily and seasonal variations in the ambient temperature for the particular geographical location. However, from the idealized curves (Fig. 4) it emerged that the actual temperature is not of prime importance, thanks to the trap distribution.

In case of the road marks, the effect of moon light can also be added to the charging by car headlamps. Depending on the phase and the elevation of the moon, this can be of similar order than the simulation in Fig. 6. However, it should be kept in mind that moon light is not omnipresent and thus not very reliable as trap filling source. As it also illuminates other objects (e.g. the non-painted road surface), the light output of the persistent phosphor will not lead to a large contrast enhancement.

Several options are available to increase the total light output. First, the phosphor can be optimized by tuning synthesis conditions, to incorporate more traps per volume of phosphor, although it is not clear yet where the fundamental limit is [25]. This optimization can be combined with a thicker phosphor layer. As beyond a certain thickness scattering losses become important, the effective thickness can be further increased by synthesizing larger, crystal-like particles, e.g. as in ceramic phosphors [17, 36], or by embedding the phosphor in

#237793 Received 9 Apr 2015; revised 9 Jun 2015; accepted 12 Jun 2015; published 23 Jun 2015

a translucent and reasonably index-matched binder, which is typically the case if the phosphor is applied as a luminous paint. Other methods to increase the light output, for instance by photonic crystals [40], are likely to add a significant cost per area.

Second, optimization of the trap depth distribution can somewhat delay the relatively high initial light output, e.g. through co-doping with other or multiple elements. Obviously, the requirements for persistent phosphors in road marks (long and steady decay) are somewhat different from the traditional emergency signage, with a focus on higher initial light output. Traps should however not be too deep, as this would lead to too many idle traps. In any case it is clear that a trap depth distribution is required to counteract the large seasonal variations in temperature.

Although the response of the $SrAl_2O_4$:Eu,Dy persistent phosphor is linear under low light levels, this is not the case during daytime illumination by the sun, as the amount of broad daylight to fill all relevant traps is of the order of a few minutes. Consequently, only a minor fraction of the available sunlight is actually used. In combination with the relatively fast initial decay, the persistent phosphor basically follows the decaying (incident) light intensity during the last hour of daylight, not fully benefiting from the strong charging capacity during the preceding hours. As outlined above, the limiting factors are thus the trap density, distribution and the (effective) phosphor thickness, which offers further roads for improvement.

## 4. Conclusion

This feasibility study showed that one of the best performing persistent luminescent phosphors, $SrAl_2O_4:Eu^{2+},Dy^{3+}$, is currently not good enough to be used in glow-in-the-dark traffic markings. The main problem is not associated with the large temperature range these phosphors should operate in, as might be expected from the fact that the available thermal energy is driving the detrapping process. The presence of a broad trap distribution in $SrAl_2O_4$:Eu,Dy leads to traps being thermally accessible in a wide temperature range. Advantageously, a larger number of traps are available during the longer winter nights.

The main problem is however related to the limited storage capacity of the phosphor, leading to an overall brightness which is too low in the later stages of the night. Further phosphor developments are therefore needed to increase the trap density in the phosphor, as well as improvements in the light extraction of thicker phosphor layers.

A final issue is the relatively strong impact of an overnight temperature drop on the brightness profile, due to a mismatch between the available thermal energy and the remaining distribution of filled traps. This is technically less straightforward to solve, although partial recharging by passing cars can ease this to some extent. Another option might be found in phosphors where at least part of the recombination is based on tunneling processes [41, 42], which are less temperature sensitive.

The conclusions presented here are to a large extent equally valid for other outdoor applications of persistent phosphors, for instance in combination with solar cells and photocatalytic processes. The methodology set out in this work is easily transferable to the evaluation of other phosphors and applications, where variable excitation conditions and temperature are the key parameters.

## Acknowledgment

The authors are thankful to the Special Research Fund (BOF-UGent) for financial support (grant n° BOF11/STA/007).

## Appendix A: Global horizontal irradiance (GHI)

The SMARTS code [33] generates the direct horizontal irradiance (DHI), being the amount of sunlight coming directly from the sun, received per unit area by a surface that is horizontal to the earth's surface. In addition, scattered sun light can also reach the surface. This is included

#237793 Received 9 Apr 2015; revised 9 Jun 2015; accepted 12 Jun 2015; published 23 Jun 2015

in the global horizontal irradiance (GHI), which includes both sunlight coming directly from the sun (DHI) and sunlight that has been scattered diffusely by the atmosphere. Note that in this simulation we limited ourselves to horizontal surfaces. For other applications, where the receiving surface is tilted, other parameters are required. From the DHI and GHI spectra obtained at various times during a day, the fraction $f_{\lambda<450nm}$ of the irradiance corresponding to light with $\lambda < 450nm$ was calculated.

The evolution of $f_{\lambda<450nm}$ for DHI and GHI is shown in Fig. 7 for a summer and winter day in Ghent (latitude of 51°N). For the DHI, $f_{\lambda<450nm}$ is maximal when the sun is at its highest elevation, while it is very low around sunrise and sunset. At these moments of the day, the sunlight travels a relatively longer distance through the atmosphere. Almost all short wavelength light is absorbed or scattered and does not contribute to the DHI anymore. The scattered light is not completely lost, as part of it can still reach the earth's surface as diffuse horizontal irradiance thereby contributing to the GHI. From sunrise to sunset, $f_{\lambda<450nm}$ for the GHI remains approximately 12%, but around sunrise and sunset a cat ear feature can be noticed . These features are a short period of elevated $f_{\lambda<450nm}$ values and can be attributed to the strong scattering of short wavelength light by the atmosphere. At sunrise (or sunset), when the sun is still (partly) below the horizon, there is hardly any DHI and the GHI is dominated by diffuse light due to scattering in the atmosphere. As the scattered component consists of particularly short wavelength light, $f_{\lambda<450nm}$ for GHI is suddenly higher at these moments of the day, although the total incident light intensity is fairly limited at these moments [43].

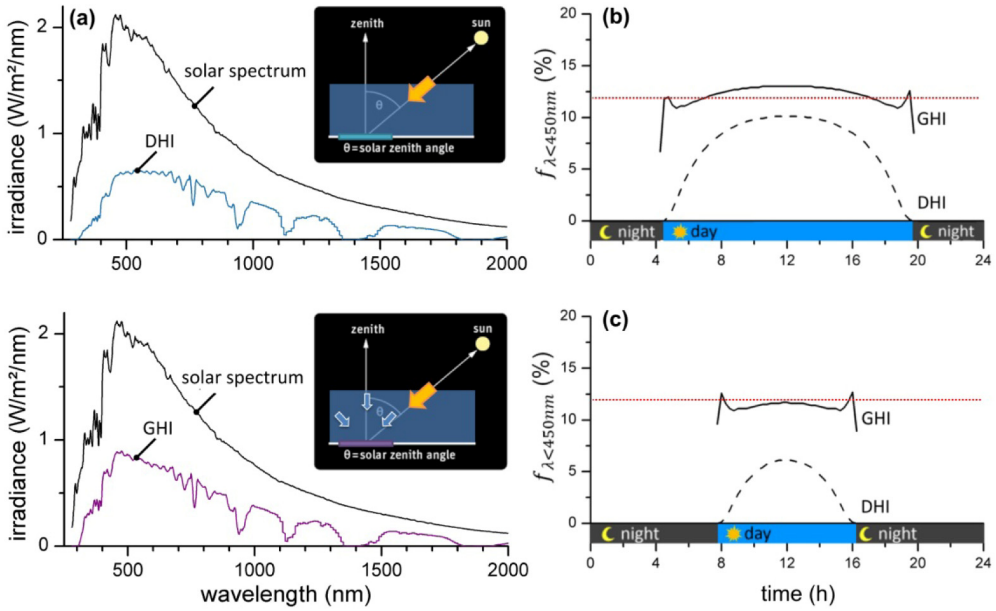


Fig. 7. (a) Effect of atmospheric absorption and scattering on the extraterrestrial solar spectrum. The upper image shows a direct horizontal irradiance (DHI) spectrum, the lower image shows a global horizontal irradiance spectrum (GHI). Both spectra are generated using SMARTS for a summer's day at 16:30 at a latitude of 45°N. Fraction of the direct horizontal irradiance (DHI) and the global horizontal irradiance (GHI) corresponding to light with $\lambda <$ 450nm calculated with SMARTS for June 21 (b) and December 21 (c) in Ghent, Belgium (latitude 51°N) . The red dotted line in (b) and (c) indicates a constant fraction of 12% (see text).

In principle, a certain fraction of the long wavelength light of the solar spectrum can also lead to photostimulation, and thus detrapping [44]. However, the cross-section of this photostimulation process is generally much smaller than for the charge trapping induced by the short wavelength component. Consequently, the photostimulation was not included

#237793 Received 9 Apr 2015; revised 9 Jun 2015; accepted 12 Jun 2015; published 23 Jun 2015

explicitly in this work. A similar reasoning applies for the additional charging by the car headlamps.

**Appendix B: Charging by headlamps**

Calculating how intense the traffic markings are lit by passing cars is not straightforward, as the intensity profile produced by the headlamps is by no means uniform. A low beam light distribution has to satisfy three main aspects. i) it should provide a homogeneous basic illuminance distribution at the road surface, ii) a spot with higher brightness in front of the car should cover the distant range of the road and iii) glaring of the oncoming traffic should be avoided. Headlamps are designed in such a way that they collect the emitted light from the light source (halogen-lamp, HID, LED, etc) and redirect it into the proper spatial distribution. Based on a typical intensity distribution of headlamps on a test wall [45], the corresponding illuminance profile was projected onto a horizontal road surface (Fig. 8).

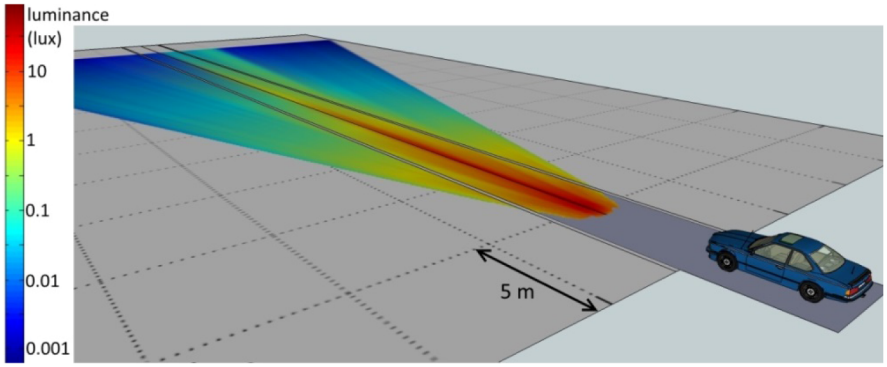


Fig. 8. Projection of a typical illuminance profile of headlamps onto the road surface.

It confirms that the illuminance distribution at the road surface is far from uniform and is most intense in the zone right in front of the car. With these data, the illumination of a traffic marking parallel to the driving direction can be estimated. Obviously this depends strongly on the position of this line relative to the car. For a traffic marking line with a width of 0.2m and length of 60m, integrating the luminous flux on this surface area yields a value of about 83lumen. So on average, the illuminance will be around 7lux. This rather low value already suggests that additional charging by a single car is limited. The effect is verified by introducing additional charging during the afterglow measurements (Fig. 7). Taking a luminous efficacy rate (LER) of 300 lum/W for the emission spectrum, approximately 0.3W of white light will be irradiated on the $12m^2$ traffic marking line. Furthermore, only a fraction of 10% of the incident light on the traffic marking line is useful for charging of $SrAl_2O_4:Eu^{2+},Dy^{3+}$. This is an upper limit, considering the fraction with $\lambda$ <450nm, being useful for the investigated phosphor. The majority of cars is equipped with tungsten-halogen headlamps for which the spectral distribution does not contain much blue or UV light. For cars with xenon headlamps - which are actually metal-halide lamps containing xenon - the fraction of blue light is somewhat larger. Most recent technology uses LEDs for headlamps. White light LEDs are commonly based on a blue LED (peak wavelength of 450 to 460nm) and one or more conversion phosphors [46]. These LED headlamps often have higher colour temperatures [39], leading to a larger fraction of blue light. The limited band width of the pumping LEDs yields a fairly large useful fraction for charging $SrAl_2O_4:Eu,Dy$. Consequently, estimating the useful fraction at 10% is justified.

#237793 Received 9 Apr 2015; revised 9 Jun 2015; accepted 12 Jun 2015; published 23 Jun 2015